Electrochemical behavior of Bi 4 B 2 O 9 towards lithium-reversible conversion reactions without nanosizing

Florian Strauss, Gwenaëlle Rousse, Dmitry Batuk, Mingxue Tang, Elodie Salager, Goran Dražić, Robert Dominko, Jean-marie Tarascon

Electrochemical behavior of $Bi_4B_2O_9$ towards lithium – reversible conversion reaction without nanosizing

Florian Strauss[a,b,c,#], Gwenaëlle Rousse[b,c,d,e], Dmitry Batuk[b,f], Mingxue Tang[g,e,+], Elodie Salager[g,e], Goran Dražić[a], Robert Dominko[a,c], Jean-Marie Tarascon[b,c,d,e,*]

[a] National Institute of Chemistry, Hajdrihova 19, SI-1000 Ljubljana, Slovenia

[b] UMR 8260 "Chimie du Solide et Energie", Collège de France, 11 Place Marcelin Berthelot, 75231 Paris Cedex 05, France

[c] ALISTORE – European Research Institute, 33 rue Saint-Leu, Amiens 80039 Cedex, France

[d] UPMC Univ Paris 06, Sorbonne Universités, 4 Place Jussieu, F-75005 Paris, France

[e] Réseau sur le Stockage Electrochimique de l'Energie (RS2E), FR CNRS 3459, 80039 Amiens Cedex, France

[f] EMAT, University of Antwerp, Groenenborgerlaan 171, B12020, Antwerp, Belgium

[g] Université d'Orléans, CNRS, CEMHTI UPR3079, 1D avenue de la recherche scientifique, 45071 Orléans Cedex 2, France

Abstract

Conversion type materials, in particular metal fluorides, have emerged as attractive candidates for positive electrodes in next generation Li-ion batteries (LIB's). However, their practical use is being hindered by issues related to reversibility and large polarization. To minimize these issues, few approaches enlisting the anionic network have been considered. We herein report the electrochemical properties of a bismuth oxyborate $Bi_4B_2O_9$ and show that this compound reacts with lithium via a conversion reaction leading to a sustained capacity of 140 mAh/g when cycled between 1.7 and 3.5 V vs. Li^+/Li^0 while having a surprisingly small polarization (~300 mV) in presence of solely 5% in weight of carbon additive. These observations are rationalized in terms of charge transfer kinetics via complementary XRD, HRTEM and NMR measurements. This finding demonstrates that borate based conversion type materials display rapid charge transfer with limited carbon additives, hence offering a new strategy to improve their overall cycling efficiency.

Introduction

Lithium ion batteries (LIB's) play an important role in powering portable electronics. Moreover, they are conquering the automotive market and stand as a contender for stationary energy storage.[1,2] Presently, the state of the art materials for LIB's are based on intercalation compounds which rely either on cationic (e.g. $LiCoO_2$, $LiFePO_4$) or cumulative cationic/anionic (Li-rich layered oxides $Li_{1+x}M_{1-x}O_2$, M = Mn, Co, Ni) redox processes as recently reported.[2] This latter finding has enabled the feasibility to reach 2 e^- per d-metal as for β-Li_2IrO_3.[3] Nevertheless, electrodes functioning via conversion reactions were first mentioned back in the 1978's[4] and fully demonstrated in 2000 for 3d transition metal oxides (CoO, NiO…).[5] These reactions, demonstrated for binary metal oxides, were latter on generalized to metal sulfides, nitrides, halides, phosphides. They enlist upon electrochemical reduction a decomposition of the binary phases into metal nanoparticles embedded into a matrix of Li_2O, Li_2S, Li_3P, according to the reaction scheme below (in the case of oxides). [6,7]

$$M_xO_y + 2y\,e^- + 2y\,Li^+ \leftrightarrow x\,M^0 + y\,Li_2O \qquad (1)$$

Such conversion reactions can deliver capacities exceeding 1000 mAh/g as compared to 280 mAh/g for the best insertion electrodes, with potentials ranging from 0.2 V to 3 V depending on the nature of the anion. The more electronegative the anion is, the higher the redox potential. This explains the use of 3d-metal based fluorides as positive electrodes. However, the capacity benefits offered by these conversion electrodes are negated by a large irreversible capacity (~ 25%) during the first cycle and poor energy efficiency associated with a large polarization between charge and discharge. Additionally, in presence of highly insulating compounds (fluorides), there is a need to prepare nano-composite electrodes heavily loaded in carbon (~ 30%) to ensure a proper electronic conduction. This electrochemically dead carbon weight penalizes the overall electrode capacity. Nevertheless, positive electrodes based on either FeF_2, FeF_3 or BiF_3 were intensively studied together with their corresponding oxyfluorides FeOF, $Fe^{II}_{(1-x)}Fe^{III}_xO_xF_{2-x}$ and BiO_xF_{3-2x}.[8–12] The partial substitution of fluorine for oxygen was purposely done to enhance electronic conduction. Nevertheless, the large voltage hysteresis, which is known to increase from hydrides to phosphides, oxides and fluorides,[7,13] still remained an issue in terms of round trip energy efficiency. Herein, to further explore the effect of the anion electronegativity on the voltage polarization, we decided to study Bi compounds based on polyanions $(BO_3)^{3-}$. Thus, our

interest for bismuth oxyborate ($Bi_4B_2O_9$) which has been intensively studied for its optical properties.[14,15] We investigate for the first time the reaction mechanism of $Bi_4B_2O_9$ versus Li and found that this compound can deliver reversible capacities of 140 mAh/g with an average redox potential of 2.3 V and a surprisingly small polarization (~300 mV), while solely using 5 wt.% of carbon additive. Complementary galvanostatic measurements combined with *in*- and *ex situ* X-ray diffraction (XRD), high resolution transmission electron microscopy (HRTEM) and ^{7}Li nuclear magnetic resonance (NMR) spectroscopy are used to rationalize such findings.

Experimental section

a) Synthesis*:* Bismuth oxyborate $Bi_4B_2O_9$ was obtained by mixing stoichiometric amounts of bismuth oxide Bi_2O_3 (Alfa Aesar) and boric acid H_3BO_3 (Alfa Aesar 99+%) with a mortar and pestle and annealing the mixture at 600°C for 36 h in air inside an alumina crucible with one intermediate grinding. Prior to usage, Bi_2O_3 has been annealed at 700°C for 12h in air in order to decompose bismuth carbonates which partially form during storage of Bi_2O_3 in ambient atmosphere. After the heat treatment the purity of Bi_2O_3 was checked through XRD with the corresponding Rietveld refinement shown in Figure S1 indicating that Bi_2O_3 is single phase and presents a good cristallinity.

b) Electrochemical characterization: Electrochemical test were carried out in Swagelok-type cells. The active material was prepared by mixing 300 mg $Bi_4B_2O_9$ powder with 5 wt.% Carbon Super P (Alfa Aesar 99+%, BET surface area 62 m^3/g) in a stainless steel jar (10 mL volume) and one stainless steel ball (4 g) for 10 min using a SPEX high energy miller. The cells (Swagelok type) were assembled in an argon filled glove box (MBraun, Germany, O_2/ H_2O < 0.1 ppm) using a metallic lithium disc as the anode. Approximately 10 mg of the active material in powdered form was used as the cathode, separated by two sheets of glassy fiber separator soaked with LP100 electrolyte (1M $LiPF_6$ in a mixture of ethylene carbonate EC/propylene carbonate PC/dimethyl carbonate DMC 1/1/3 w/w/w). Galvanostatic charge/ discharge cycling was performed at room temperature on a VMP3 potentiostat (BioLogic S.A., Claix, France). The current was set to a specific C-rate, where a rate of 1C corresponds to a current which inserts/removes 1 Li^+ per formula unit during 1 hour.

c) Physical characterization:

X-ray powder diffraction patterns were recorded in Bragg-Brentano geometry with a Bruker D8 Advance diffractometer equipped with a copper source ($\lambda_{Cu\text{-}K\alpha1}$ = 1.54056 Å, $\lambda_{Cu\text{-}K\alpha2}$ = 1.54439 Å) and a LynxEye detector. An in-house built sample holder equipped with a Be window transparent to X-rays[16] was used for collecting the XRD patterns of the air sensitive samples. Prior to examination, the cycled powders were recovered inside the glove box, washed 3 times with DMC, dried in vacuum and filled into the sample holder without exposing them to ambient atmosphere at any time.

For *in situ* XRD experiments a similar setup as described above was used and the cell was discharged/charged using a C/10 rate corresponding to the uptake/removal of 0.1 Li per 1 hour. Patterns were continuous recorded for a 2θ range from 5 to 60° with a collection time of 1 hour for each scan.

Powder patterns were refined using the Rietveld method[17] as implemented in the FullProf program.[18] Pristine samples of $Bi_4B_2O_9$ were investigated through combined HRTEM and electron energy loss spectroscopy (EELS) analysis using a Cs probe corrected Scanning Transmission Electron Microscope Jeol ARM 200 CF equipped with Centurio EDXS system from Jeol with 100 mm^2 SDD detector and Gatan Quantum ER Dual EELS system.

To examine cycled samples of $Bi_4B_2O_9$/C, the recovered powder was grinded in a mortar and holey carbon TEM grids were dipped into the powder. To avoid exposure to air, the samples were stored and prepared for TEM in an Ar filled glovebox. A special Gatan vacuum holder was used for the transfer of the samples from the glovebox to the TEM in order to avoid air exposure. Electron diffraction (ED) data, EDX spectroscopy elemental maps and high resolution transmission electron microscopy (HRTEM) images were acquired on an FEI Osiris microscope operated at 200 kV and equipped with a Super-X EDX detector.

^{7}Li magic-angle-spinning (MAS) NMR experiments were performed on a Bruker Avance III spectrometer in a 4.7 T magnetic field with a ^{7}Li Larmor frequency of 77.8 MHz. Electrodes were packed into 1.3 mm rotors inside an Ar-filled glovebox and spun at a MAS rate of 62.5 kHz (unless specifically stated elsewhere) under N_2 protection. The recycle delay was varied from 8 to 20 s to make sure that the excited spins were fully relaxed. The 90^o pulse length was calibrated as 1.38 µs. LiCl(s) with a ^{7}Li chemical shift at 0 ppm was used as the shift reference. The spectra were calibrated by samples weight and number of scans.

Results and Discussion

a) Structural characterization

The resulting yellowish $Bi_4B_2O_9$ powder made at 600°C consists of agglomerated crystals whose size ranges from 5 to 10 µm (Figure 1, inset). The corresponding XRD pattern and the Rietveld refinement recorded for a 2θ ranging from 5 to 100° are shown in Figure 1. All peaks could be indexed in a monoclinic space group $P\,2_1/c$ with the unit cell parameters a = 11.1153(8) Å, b = 6.6324(1) Å, c = 11.0447(3) Å, β = 91.0465(3)° and V = 814.009(4) Å^3, as reported in literature.[14,19] All atoms are placed in general positions 4*e* with four crystallographic sites for bismuth, two for boron and nine for oxygen atoms. The final atomic positions are given in Table S1.

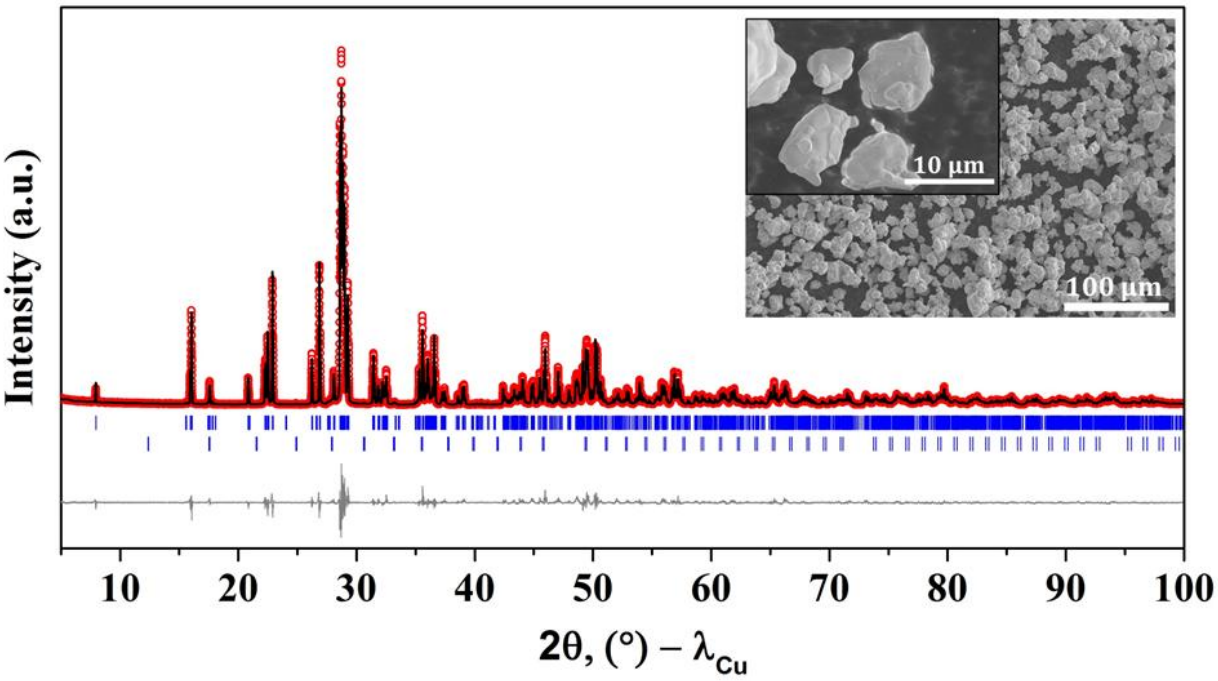

Figure 1: Rietveld refinement of $Bi_4B_2O_9$ and representative SEM images of the powder obtained after the solid-state synthesis. The red crosses, black continuous line and bottom green line represent the observed, calculated, and difference patterns respectively. Upper and lower vertical blue tick bars are the Bragg positions of $Bi_4B_2O_9$ and the impurity phase $Bi_{24}B_2O_{39}$ (0.4 wt.%).

The atomic arrangement within the unit cell is shown in Figure 2. Boron is trigonal planar coordinated by oxygen forming regular BO_3^{3-} triangles (average B-O bond distance

1.3396 Å) which are stacked in parallel along the *b*-axis (Figure 2). Bismuth is four- and five-fold coordinated by oxygen forming asymmetric truncated BiO_4 and BiO_5 polyhedra with Bi-O distances ranging from 2.150 to 2.492 Å. Note that three crystallographic independent oxygen atoms (denoted O1, O2 and O4) are solely connected to Bi atoms and are not part of borate groups, hence $Bi_4B_2O_9$ can be called an oxyborate.

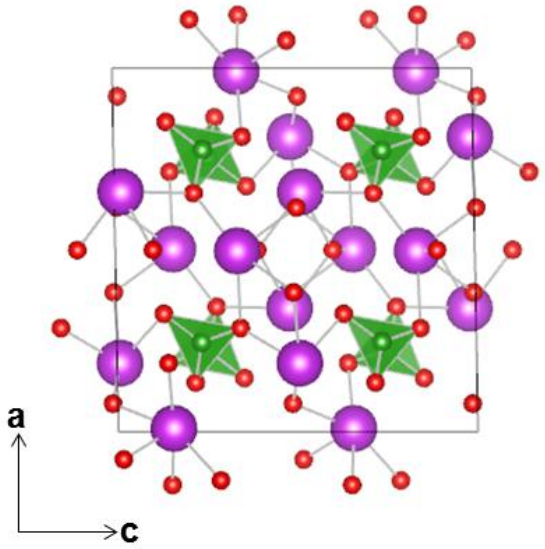

Figure 2: Structure of $Bi_4B_2O_9$ projected along the b-axis. Bismuth, boron and oxygen are drawn in purple, green and red respectively.

Figure S2a shows a typical XRD pattern of the $Bi_4B_2O_9$/C composite after ball milling with carbon black for 10 minutes. There is a slight broadening of the Bragg peaks pertaining to $Bi_4B_2O_9$, indicative of a decrease in the sample particle size. Rietveld refinements were undertaken with an isotropic size parameter (Scherrer formula) as a refinable parameter. Results indicate a decrease in the average crystallite size from ~6 µm to ~680 nm for the pristine and milled $Bi_4B_2O_9$, respectively. This was further confirmed by electron microscopy of the carbon/active material composite as shown in Figure S2b.

b) Electrochemistry

A typical voltage composition curve in galvanostatic mode between 1.0 and 3.5 V together with the corresponding derivative plot is shown in Figure 3 and capacity retention is shown in Figure 4. The initial reduction corresponds to the reaction of 12 Li^+ with one mole of $Bi_4B_2O_9$. Such a Li uptake is associated with two different voltage regimes. At the beginning of the discharge, a flat plateau at 1.8 V is visible concomitant with the uptake of 8 Li^+, followed by an S-shape domain centered around 1.4 V and corresponding to the uptake of 4 Li^+. On following charge, 8 Li^+ can be extracted via two different voltage regimes located at ~1.6 and ~2.5 V (Figure 3b). On subsequent cycling, the initial reduction processes around 1.8 and 1.4 V become reversible with the former one shifted up to 2.2 V through the subsequent discharges (Figure 3b). This potential difference between the initial and following discharge is typically observed for conversion type materials since different reaction pathways occur during the initial and subsequent reductions. The potential drop is larger during the first discharge because of the higher activation energy needed to trigger the conversion reaction as explained in the first seminal paper on this topic.[5] After this formation step, the second and subsequent discharges will be kinetically less limited owing to the nano character of the formed composite, hence the discharge potential is increased.[20] An irreversible loss in capacity between the first and second discharge (about 33%) is observed and the initial capacity decays of about 50% within the first 3 cycles (Figure 4).

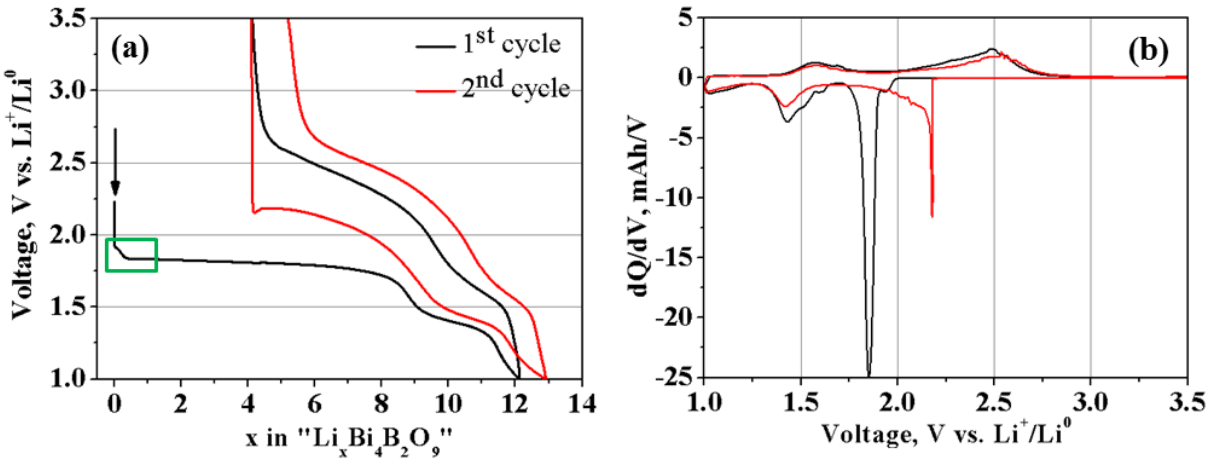

Figure 3: (a) Voltage-composition curve of $Bi_4B_2O_9$ versus Li^+/Li^0 cycled at a C/10 rate between 1.0 and 3.5 V and (b) the corresponding derivative plot.

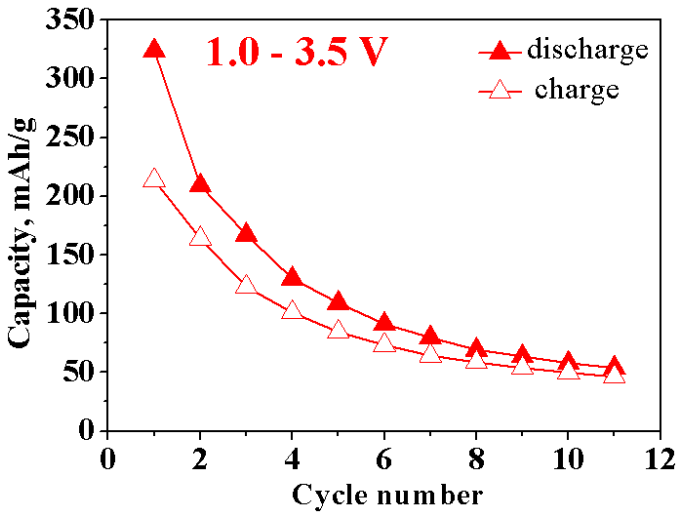

Figure 4: Capacity retention of $Bi_4B_2O_9$/Li half-cell cycled between 1.0 and 3.5 V with a C/10 rate.

The complete reduction of $Bi_4B_2O_9$ via a conversion reaction would require, according to reaction 2, the uptake of 12 Li^+ and 12 e^- to form elemental Bi, lithium oxide Li_2O and lithium borate Li_3BO_3. This number is in good agreement with the amount of reacted Li deduced from the electrochemical trace down to 1.0 V (Figure 3a), however the reaction is only partially reversible as not the entire Li could be extracted upon subsequent charge to 3.5 V; a main characteristic of conversion reaction which always shows large irreversibility between first discharge and first charge.[5]

$$Bi_4B_2O_9 + 12\,Li^+ + 12\,e^- \leftrightarrow 3\,Li_2O + 2\,Li_3BO_3 + 4\,Bi^0 \qquad \textbf{(2)}$$

X-ray diffraction measurements upon cycling were realized to examine Li-driven structural changes in $Bi_4B_2O_9$ using a homemade cell equipped with a Be window transparent to X-rays.[16] We initially scrutinized the sloping voltage region at the beginning of the initial reduction centered around 1.9 V (green rectangle, Figure 3a). The collected *in situ* XRD patterns together with the corresponding electrochemical trace are presented in Figure 5. One can notice constancy in the intensity of the reflections (zoom Fig. 5b) and that neither a shift of the pristine reflections nor an appearance of a new phase was observed. However the onset of an insertion prior to a conversion reaction has been observed in literature for several other conversion materials.[21–23] Although a possible Li contribution in the XRD

patterns should be heavily masked by Bi (Z = 83), Li intercalation would lead to a change in lattice parameters. However the refined lattice parameters based on the *in situ* recorded XRD patterns are shown to be constant (Figure S3) for a Li uptake for x = 1, hence a Li insertion process into $Bi_4B_2O_9$ can be excluded.

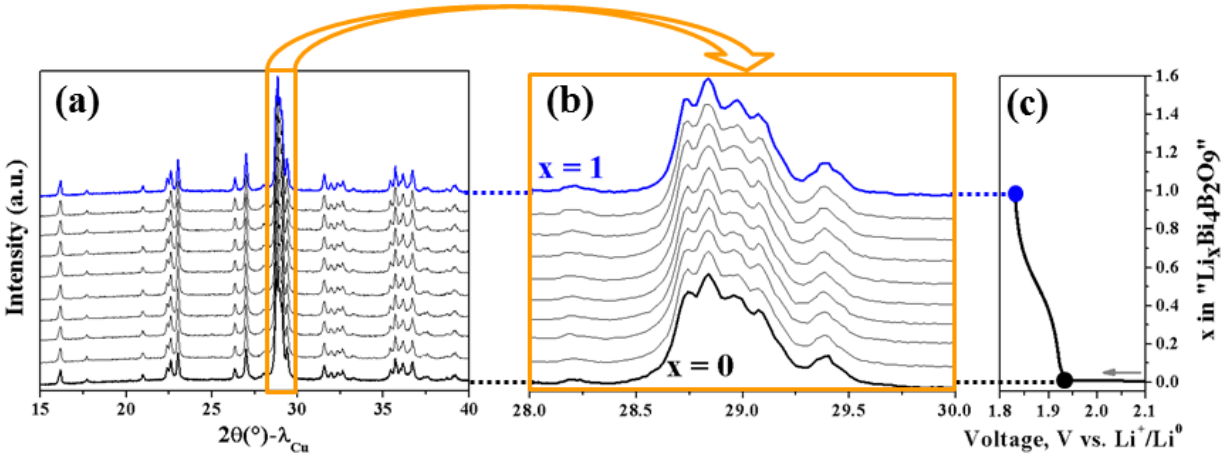

Figure 5: *In situ* XRD of a $Bi_4B_2O_9$/Li half-cell cycled at C/10 for the uptake of 1 Li^+. (a) Global view of the overall scanned 2θ angle, whereas in (b) a magnification of the main reflections is shown and in (c) the corresponding electrochemical trace is presented.

To pin down the origin of the process occurring at the beginning of the initial discharge, $Bi_4B_2O_9$/Li cells were discharged with different C-rates, ranging from 1C to C/100 (Figure S4a). When the C-rate decreases, we note a more defined pseudo-plateau around 1.95 V which disappears for rates higher than C/5 indicating kinetic limitations of this process. Since *in situ* XRD ruled out a Li^+ insertion process, we hypothesize that the initial pseudo-plateau region is most likely related to surface reactions. This hypothesis is confirmed by comparing the initial discharge between a ball-milled and handground $Bi_4B_2O_9$/C composite with namely an increase (Figure S4b) of the initial sloping region from x = 0.25 to x = 1 for the ball milled samples which present the greatest surface area.

Interestingly, HRTEM (Figure 6a) provides evidence for the presence of a ~3 nm thick amorphous surface layer on pristine $Bi_4B_2O_9$ particles, which is mainly made up of amorphous bismuth oxide Bi_xO_y (Figure 6b, c). This observation suggests the removal of some oxygen from the amorphous surface layer during the sloping initial voltage region to lead to the formation of Li_2O and an oxygen deficient surface Bi_xO_{y-z}. In favor of such an

explanation let us recall that the voltage-composition profile of $Bi_4B_2O_9$ versus Li presents a profile alike the one obtained during the electrochemical reduction of BIMEVOX phases ($Bi_4V_2O_{11}$, $Bi_{3.6}Pb_{0.4}V_2O_{11-y}$, $Bi_4V_{1.8}Cu_{0.2}O_{11-y}$),[24,25] which has been previously reported as being nested in an oxygen removal process of the pristine material upon reduction, yielding to $Bi_4V_2O_{10.66}$ and an amorphous Li_2O shell formed around the particles.[24] Thus we assume that a similar reaction takes place in the case of $Bi_4B_2O_9$. Note that we were unfortunately not able to any further insights through TEM analysis, due to the beam sensitivity of the milled $Bi_4B_2O_9$ particles once discharged.

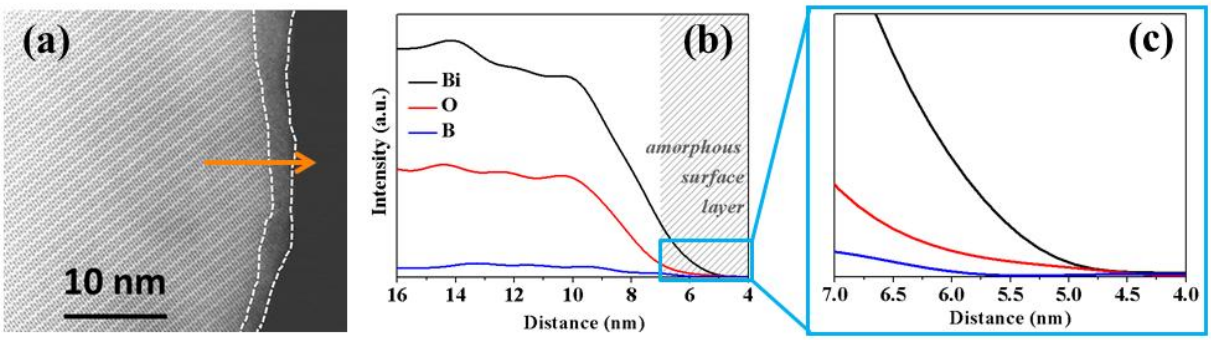

Figure 6: (a) STEM picture of a $Bi_4B_2O_9$ particle as synthesized where an amorphous surface layer is highlighted between the two white dashed lines. (b) EELS analysis along the orange arrow indicated in (a) where the amorphous surface layer is indicated with the grey shaded area and (c) shows a zoom of that region.

The *in situ* XRD patterns and the corresponding electrochemical trace when the discharge is further continued down to 1.7 V are shown in Figure S5. There is a decrease in the intensity of the pristine reflections to the expense of a broad bumpy background for angles greater than 22.5° 2θ (Figure S6a). This is indicative of the appearance of some diffuse scattering, implying a Li-driven amorphization of the "$Li_xBi_4B_2O_9$" material.

Additional *ex situ* XRD patterns were recorded for two different samples that have been discharged to 1.0 V and charged back to 3.5 V (Fig. S6b). The powders, prepared by disassembling cycled cells inside the glove box, were recovered, washed twice with DMC and dried under vacuum prior to measurement. The X-ray powder pattern collected at 1.0 V is featureless with the exception of some weak reflections over the 28°- 32° 2θ region, implying a pronounced amorphization of the "$Li_xBi_4B_2O_9$" material. These weak features are still present in the XRD pattern fully charged (3.5 V) sample, hence indicating that they are

likely due to traces of non-electrochemically connected pristine materials. On subsequent cycling, we noticed that the amorphous nature of the electrode composite remains.

To get further insights into the Li-driven structural/morphological changes on the partly reduced or oxidized samples, we performed TEM measurements. A representative image of $Bi_4B_2O_9$ reduced to 1.0 V (Figure 7) shows the appearance of nanoparticles embedded in an amorphous matrix. The selected area electron diffraction (SAED) analysis of the nanocomposite (Fig. 7b) shows characteristic diffraction rings/spots characteristic of elemental Bi. Note that due to their very small size (~5 nm) and the resulting large peak broadening, we could not identify Bi reflections in the corresponding XRD pattern at 1.0 V (Figure S6b) that shows a high background due to the presence of amorphous phases. The identification of Bi nanoparticles was further confirmed by EDXS. However, we could not probe the distribution of Li and B, since EDX analysis cannot spot light elements. Additionally, we observed a strong agglomeration of the Bi nanoparticles (Figure 7c) after discharge to 1.0 V. Lastly, Bi particles could be also be spotted with SAED in the recharged 3.5 V sample (Figure S7a), even though the diffraction rings are less pronounced as compared to the discharge sample indicative of a lower amount of Bi present in the charged sample. Overall the results obtained from TEM at this stage explain the poor reversibility on subsequent cycling due to kinetic limitations associated to particles coarsening and agglomeration of Bi. However, we could not reconfirm the formation of $Bi_4B_2O_9$ since the collected SAED patterns reveal barely detectable rings besides the one denoted to Bi (Figure S7b), indicative of the amorphous nature of the recharged phase.

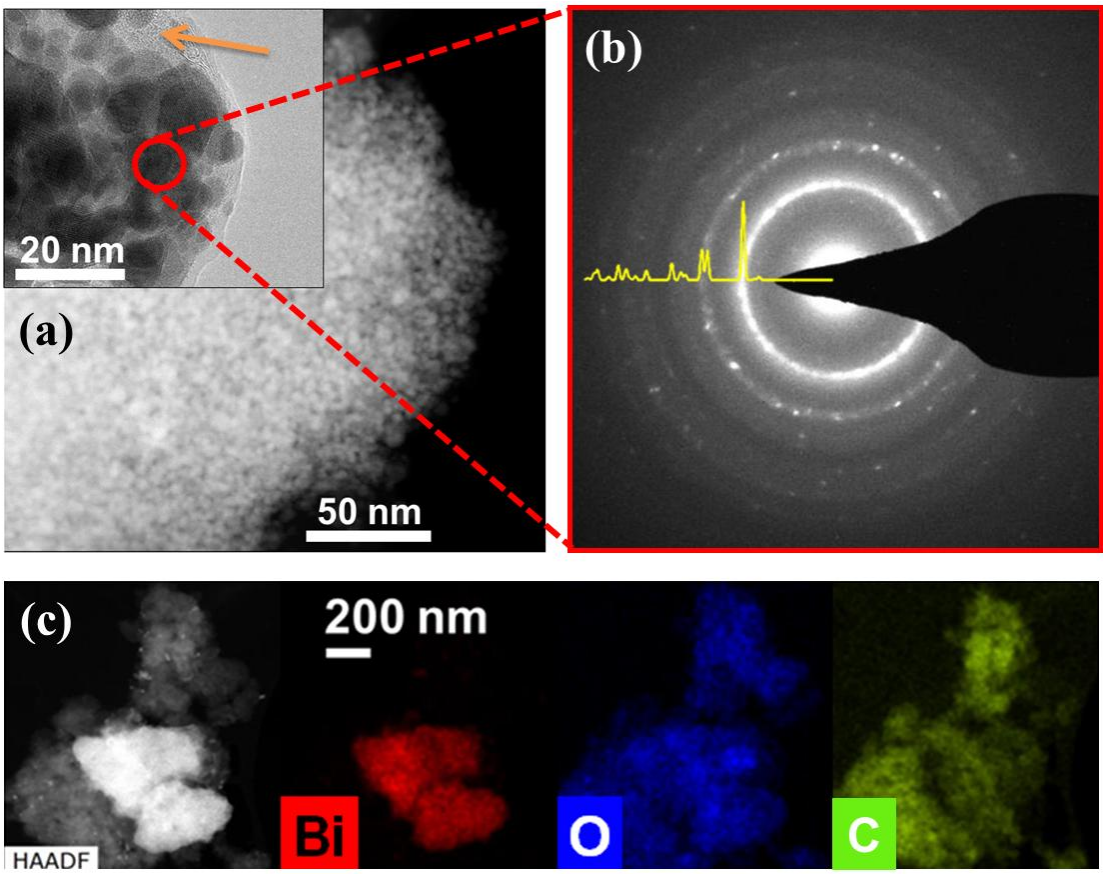

Figure 7: (a) TEM image of a sample discharge to 1.0 V. The orange arrow in the inset is indicating the bright amorphous matrix consisting of Li_2O/ Li_3BO_3. (b) SAED image of the composite. (c) TEM image and the corresponding elemental maps for Bi, O and C given in red, blue and green respectively.

In short, we could demonstrate through TEM the partial reversible formation of elemental Bi upon the electrochemical reduction of $Bi_4B_2O_9$ versus Li. However the formation of Li_2O and Li_3BO_3 as stated in the reaction scheme (equation 2) could not be evidenced yet due to their most likely nanocrystalline/amorphous nature, similar as observed in the case of transition metal borates.[26] As an attempt to circumvent this issue, Nuclear Magnetic Resonance (NMR), which is a suitable tool for probing local structures[27–30] and their evolvement upon electrochemical cycling was used taking advantage of the ^7Li nuclei.[31,32] Well-resolved ^7Li NMR measurements were performed for $Bi_4B_2O_9$ samples discharged to 1 V and 1.7 V prior to recharge each of them to 3.5 V as shown in Figure 8. Only one sharp resonance locating at 0 ppm is observed for all the chosen electrodes, indicating that both of the formed products Li_2O and Li_3BO_3 are diamagnetic. The residual interaction are observed by obvious spinning side bands (SSBs) cover over ~1600 ppm even

under fast spinning, indicating partially disordered structure and strong dipolar interaction within these electrodes, in accordance with the amorphous/nanocrystalline nature of the Li_2O/Li_3BO_3 matrix (Figure 8a, inset). Moreover, by integration of the ^7Li NMR signal for both 1 and 3.5 V samples, we could deduce a ^7Li signal 3 times larger for 3.5 V sample as compared to the 1 V sample, which is consistent with the corresponding Li content of ~12 and ~4 in the 1.0 and 3.5 V samples, respectively (Figure 3a). Altogether, these observations confirm the overall reaction scheme proposed in equation 2.

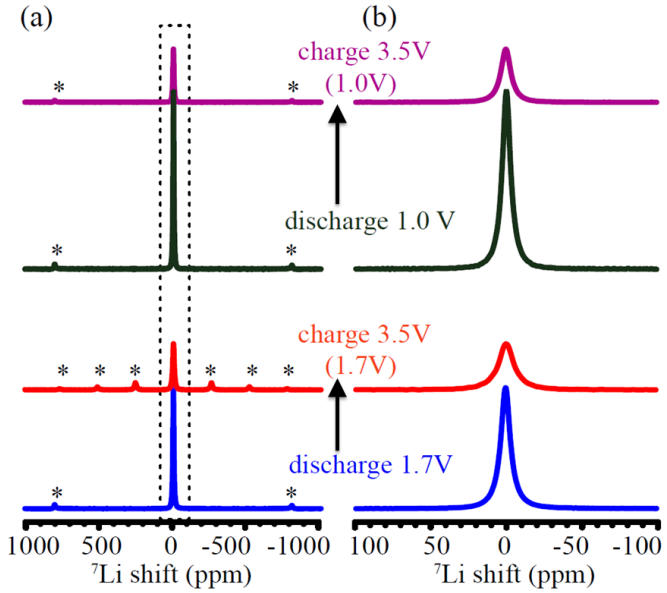

Figure 8: (a) ^7Li MAS NMR spectra of $Li_xBi_4B_2O_9$ electrodes at different states of charge/ discharge and (b) the enlargement of the framed region are shown in (a). The asterisks marked in (a) demonstrate the SSBs. Spectra are calibrated to mass weight of electrodes and number of scans.

Finally, the existence of two plateaus at 1.8 and 1.4 V in the discharge curve (Figure 3) suggests step-wise reactions, which are difficult to fully study because of the amorphous/nanocrystalline nature of the formed products. Nevertheless, previous studies on 3d-metal borates have indicated the formation of Li_3BO_3 at redox potentials depending upon the nature of the 3d-metal,[26] while reactivity of δ-Bi_2O_3 and α-Bi_2O_3 vs. Li occurs via conversion reactions at 1.8 and 1.2/1.4V respectively.[8,33] Note that this is nearly the same redox potentials we have measured when discharging $Bi_4B_2O_9$ vs. Li. Although quite

speculative, it is thus tempting to hypothesize that during the conversion of $Bi_4B_2O_9$ there is first the conversion of the borate leading to the formation Li_3BO_3 and Bi, and simultaneously to the growth of the two δ and α Bi_2O_3 polymorphs. Both polymorphs will undergo conversion reactions at 1.8 and 1.4 V respectively (accompanied with the formation of Li_2O and Bi), before all $Bi_4B_2O_9$ is converted, with the length of the different plateaus corresponding to the relative ratio of these polymorphs. Although we do not have evidence for the existence of Bi_2O_3 from electron microscopy at present, our hypothesis of starting with the formation of Li_3BO_3 and then Li_2O seems to be reasonable, and similar observations have been made for the bismuth oxyfluoride system. This system was shown to react with Li via a conversion reaction, but the conversion of the fluoride occurs first, followed by the conversion of the as-formed bismuth oxide.[8]

At this stage a legitimate question deals with the poor reversibility of the reduction process when the cycling spans over the 1 to 3.5 V voltage range and whether it could be improved by limiting the potential window. To check this point, $Bi_4B_2O_9$/Li half cells were cycled between 1.7 and 3.5 V (Fig. 9a). The voltage-composition curve shows, aside the initial step voltage previously discussed, a discharge plateau at 1.8 V corresponding to the uptake of 8 Li^+. On the subsequent charge, which shows an S-type voltage profile, only 5 out of the 8 uptake Li^+ ions can be released, hence leading to an irreversible capacity of ~35 %. Note that the following discharge does not follow the first one and this is indicative of a conversion reaction. Once the first cycle is achieved, the average potential of the cell is about 2.3 V with a sustained reversible capacity of ~140 mAh/g for several cycles prior the appearance of a noticeable fading (Figure 9b). This strongly improved capacity retention by limiting the voltage window from 1.0 – 3.5 V to 1.7 – 3.5 V, does not come as a total surprise as it is known that by increasing the discharge cutoff potential Bi agglomeration is minimized (Figure S8a versus Figure S8b, and Figure 7).[34] Moreover by cycling $Bi_4B_2O_9$ over a high potential window, parasitic side reactions such as reductive electrolyte decomposition are not as pronounced as for potentials < 1.7 V. This continuous decomposition most likely leads to the formation of an insulating organic layer, propagating particle separation/ coarsening and thus deteriorating charge transport throughout the composite leading to an increase in voltage polarization upon cycling (Figure 10a).[35,36] Interestingly, ^{7}Li NMR measurements for electrode samples discharged 1.7 and recharged to 3.5 V (Figure 8) reveal the existence of Li_2O and Li_3BO_3 . Again the signal integration for the discharged sample (1.7 V) is about 3

times greater than for the charged one (3.5 V), consistent with the Li content deduced from the voltage composition curve (Figure 9a).

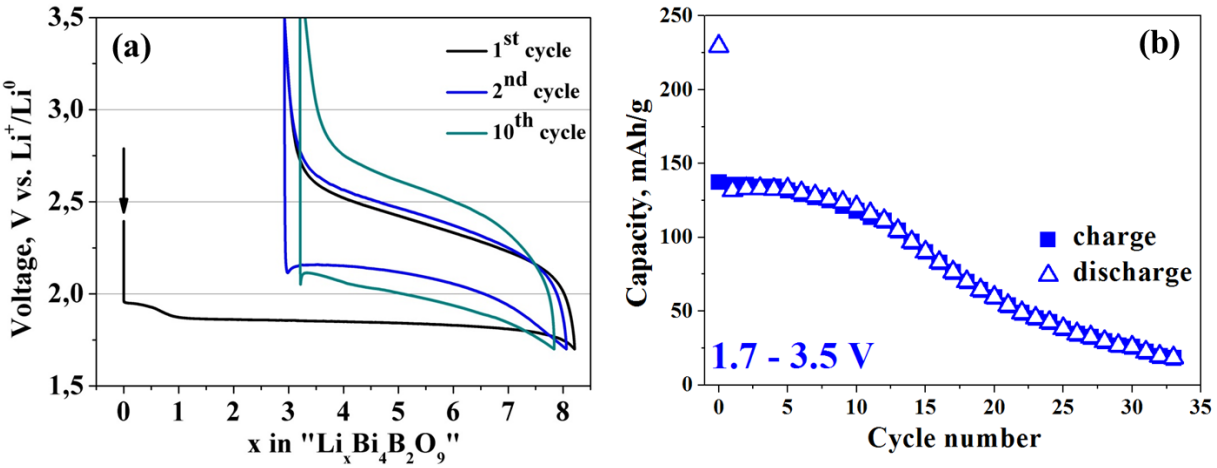

Figure 9: (a) Voltage-composition curve of $Bi_4B_2O_9$ versus Li cycled at a C/10 rate between 1.7 and 3.5 V and (b) the corresponding capacity retention.

Two other important experimental findings are worth mentioning regarding the cycling performances of $Bi_4B_2O_9$/Li cells. They are *i)* the ability to reversibly cycle $Bi_4B_2O_9$ powders made of macroscopic particles with only 5 wt.% carbon additive and *ii)* the small cycling hysteresis around 300 mV, while usually conversion reaction electrodes require at least 20% of carbon and show voltage polarization greatly larger. The origin of such a difference is most likely rooted in the presence of a ~3 nm thick amorphous surface layer onto the $Bi_4B_2O_9$ particles, as deduced by HRTEM (Figure 6a), which is mainly made up of amorphous bismuth oxide (Figure 6b, c). Since it is well known that non-stoichiometric metal oxides, namely Bi-oxides can promote electronic conductivity,[37–39] we can hypothesize that this layer is responsible for enhanced charge transfer kinetics, enabling electronic conducting, hence accounting for the use of solely 5 wt.% of conductive carbon additive. This hypothesis is supported by the fact that $Bi_4B_2O_9$ as synthesized could be electrochemically cycled without any conducting additive between 1.0 and 3.5 V (Figure S10), although the reversibility is very poor once the material is electrochemically grinded, due to the loss of electronic percolation throughout the formed composite composed of insulating Li_2O and Li_3BO_3 phases. The positive effect of this amorphous surface layer on the electrochemical activity of $Bi_4B_2O_9$ is raising questions about its origin and how to control its formation.

Boron species (in particular boron oxide B_2O_3) are well known to be volatile at elevated temperatures,[40–42] hence the feasibility to form a boron deficient surface layer during the prolonged annealing treatment.

Turning the relative small voltage polarization observed for $Bi_4B_2O_9$, it is of the same amplitude as displayed by other borates which react towards Li via a conversion reaction. [26,43] Although the origin of such polarization is not fully understood, theoretical studies and recent experimental work on the conversion reaction of Co_3O_4 with Na,[44] suggest that it is associated to different thermodynamic paths for charge and discharge that are correlated to the difference in ionic mobilities between Li and displaced ionic species (herein B, O, Bi).[23,44,45] Borate species may thus play a crucial role as network former leading to a continuous amorphous matrix promoting enhanced ionic conductivity as observed for a wide range of borate glasses.[46–49]

Conclusion

We have reported that $Bi_4B_2O_9$ reversibly reacts versus Li via a conversion-type reaction leading to the formation of Bi nanoparticles surrounded by an amorphous matrix composed of Li_2O and Li_3BO_3, as deduced by combined XRD, TEM imaging and ^{7}Li NMR spectroscopy. We found this process to be reversible by limiting the cycling voltage range to 1.7 – 3.5 V so that capacities of 140 mAh/g can be achieved at an average potential of 2.3 V. Moreover, bearing in mind that the density of $Bi_4B_2O_9$ is large (8.17 g/cm^3), we can reach a volumetric energy density of 2819 Wh/L. Remarkably such values can be achieved with both a small polarization (300 mV) and the addition of solely 5 wt.% carbon, which is quite unusual for conversion type cathode materials. Such a finding is rationalized through the appearance of an amorphous nanometer thick Bi-oxide rich surface layer during the synthesis of $Bi_4B_2O_9$ which in particular enhance electronic transport. Having point out the importance of surface morphology and benefit of the borate species towards the electrochemical properties of conversion type electrode materials, it now pertains to see if this concept can be applied to other borate based conversion materials.

Author information

Corresponding Author

* E-mail: jean-marie.tarascon@college-de-france.fr

Notes

The authors declare no competing financial interest.

Present addresses

[#] Battery and Electrochemistry Laboratory (BELLA), Institute of Nanotechnology (INT), Karlsruhe Institute of Technology (KIT), Hermann-von-Helmholtz-Platz 1, D-76344 Eggenstein-Leopoldshafen, Germany

[+] National High Magnetic Field Laboratory, 1800 East Paul Dirac Drive, Tallahassee, Florida 32310, United States

Acknowledgement

F.S. acknowledges ALISTORE-ERI for his PhD grant. F.S. and R.D. acknowledge the financial support from the Slovenian Research Agency (research core funding No. P2-0393).

References

(1) Armand, M.; Tarascon, J.-M. Building Better Batteries. *Nature* **2008**, *451* (7179), 652–657.

(2) Sathiya, M.; Rousse, G.; Ramesha, K.; Laisa, C. P.; Vezin, H.; Sougrati, M. T.; Doublet, M.-L.; Foix, D.; Gonbeau, D.; Walker, W.; Prakash, A. S.; Ben Hassine, M.; Dupont, L.; Tarascon, J.-M. Reversible Anionic Redox Chemistry in High-Capacity Layered-Oxide Electrodes. *Nat. Mater.* **2013**, *12* (9), 827–835.

(3) Pearce, P. E.; Perez, A. J.; Rousse, G.; Saubanère, M.; Batuk, D.; Foix, D.; McCalla, E.; Abakumov, A. M.; Van Tendeloo, G.; Doublet, M.-L.; Tarascon, J.-M. Evidence for Anionic Redox Activity in a Tridimensional-Ordered Li-Rich Positive Electrode β-Li2IrO3. *Nat. Mater.* **2017**, *16* (5), 580–586.

(4) Besenhard Jürgen O. Chalkogenide Des As, Sb Und Bi Als Positive Elektroden in Lithium-Batterien / Chalcogenides of As, Sb and Bi as Positive Electrodes in Lithium Cells. *Z. Für Naturforschung B* **2014**, *33* (3), 279.

(5) Poizot, P.; Laruelle, S.; Grugeon, S.; Dupont, L.; Tarascon, J.-M. Nano-Sized Transition-Metal Oxides as Negative-Electrode Materials for Lithium-Ion Batteries. *Nature* **2000**, *407* (6803), 496–499.

(6) Cabana, J.; Monconduit, L.; Larcher, D.; Palacín, M. R. Beyond Intercalation-Based Li-Ion Batteries: The State of the Art and Challenges of Electrode Materials Reacting Through Conversion Reactions. *Adv. Mater.* **2010**, *22* (35), E170–E192.

(7) Wu, F.; Yushin, G. Conversion Cathodes for Rechargeable Lithium and Lithium-Ion Batteries. *Energy Env. Sci* **2017**.

(8) Bervas, M.; Klein, L. C.; Amatucci, G. G. Reversible Conversion Reactions with Lithium in Bismuth Oxyfluoride Nanocomposites. *J. Electrochem. Soc.* **2006**, *153* (1), A159.
(9) Wiaderek, K. M.; Borkiewicz, O. J.; Castillo-Martínez, E.; Robert, R.; Pereira, N.; Amatucci, G. G.; Grey, C. P.; Chupas, P. J.; Chapman, K. W. Comprehensive Insights into the Structural and Chemical Changes in Mixed-Anion FeOF Electrodes by Using Operando PDF and NMR Spectroscopy. *J. Am. Chem. Soc.* **2013**, *135* (10), 4070–4078.
(10) Kim, S.-W.; Pereira, N.; Chernova, N. A.; Omenya, F.; Gao, P.; Whittingham, M. S.; Amatucci, G. G.; Su, D.; Wang, F. Structure Stabilization by Mixed Anions in Oxyfluoride Cathodes for High-Energy Lithium Batteries. *ACS Nano* **2015**, *9* (10), 10076–10084.
(11) Chevrier, V. L.; Hautier, G.; Ong, S. P.; Doe, R. E.; Ceder, G. First-Principles Study of Iron Oxyfluorides and Lithiation of FeOF. *Phys. Rev. B* **2013**, *87* (9), 094118.
(12) Pereira, N.; Badway, F.; Wartelsky, M.; Gunn, S.; Amatucci, G. G. Iron Oxyfluorides as High Capacity Cathode Materials for Lithium Batteries. *J. Electrochem. Soc.* **2009**, *156* (6), A407–A416.
(13) Taberna, P. L.; Mitra, S.; Poizot, P.; Simon, P.; Tarascon, J.-M. High Rate Capabilities Fe3O4-Based Cu Nano-Architectured Electrodes for Lithium-Ion Battery Applications. *Nat. Mater.* **2006**, *5* (7), 567–573.
(14) Hyman, A.; Perloff, A. The Crystal Structure of Bismuth (2: 1) Borate, 2Bi2O3. B2O3. *Acta Crystallogr. B* **1972**, *28* (7), 2007–2011.
(15) Huang, H.; He, Y.; Lin, Z.; Kang, L.; Zhang, Y. Two Novel Bi-Based Borate Photocatalysts: Crystal Structure, Electronic Structure, Photoelectrochemical Properties, and Photocatalytic Activity under Simulated Solar Light Irradiation. *J. Phys. Chem. C* **2013**, *117* (44), 22986–22994.
(16) Leriche, J. B.; Hamelet, S.; Shu, J.; Morcrette, M.; Masquelier, C.; Ouvrard, G.; Zerrouki, M.; Soudan, P.; Belin, S.; Elkaïm, E.; Baudelet, F. An Electrochemical Cell for Operando Study of Lithium Batteries Using Synchrotron Radiation. *J. Electrochem. Soc.* **2010**, *157* (5), A606.
(17) Rietveld, H. A Profile Refinement Method for Nuclear and Magnetic Structures. *J. Appl. Crystallogr.* **1969**, *2* (2), 65–71.
(18) Rodríguez-Carvajal, J. Recent Advances in Magnetic Structure Determination by Neutron Powder Diffraction. *Phys. B Condens. Matter* **1993**, *192* (1), 55–69.
(19) Filatov, S. K.; Shepelev, Y. F.; Aleksandrova, Y. V.; Bubnova, R. S. Structure of Bismuth Oxoborate Bi4B2O9 at 20, 200, and 450°C. *Russ. J. Inorg. Chem.* **2007**, *52* (1), 21–28.
(20) Gillot, F.; Boyanov, S.; Dupont, L.; Doublet, M.-L.; Morcrette, M.; Monconduit, L.; Tarascon, J.-M. Electrochemical Reactivity and Design of NiP2 Negative Electrodes for Secondary Li-Ion Batteries. *Chem. Mater.* **2005**, *17* (25), 6327–6337.
(21) Bezza, I.; Kaus, M.; Riekehr, L.; Pfaffmann, L.; Doyle, S.; Indris, S.; Ehrenberg, H.; Solhy, A.; Saadoune, I. Electrochemical Lithiation/Delithiation of SnP_2O_7 Observed by in Situ XRD and Ex Situ ^{7}Li/^{31}P NMR, and ^{119}Sn Mössbauer Spectroscopy. *Phys Chem Chem Phys* **2016**, *18* (15), 10375–10382.
(22) Hwang, H.; Kim, M. G.; Kim, Y.; Martin, S. W.; Cho, J. The Electrochemical Lithium Reactions of Monoclinic ZnP2 Material. *J. Mater. Chem.* **2007**, *17* (30), 3161.
(23) Doe, R. E.; Persson, K. A.; Meng, Y. S.; Ceder, G. First-Principles Investigation of the Li−Fe−F Phase Diagram and Equilibrium and Nonequilibrium Conversion Reactions of Iron Fluorides with Lithium. *Chem. Mater.* **2008**, *20* (16), 5274–5283.
(24) Patoux, S.; Vannier, R.-N.; Mairesse, G.; Nowogrocki, G.; Tarascon, J.-M. Lithium- and Proton-Driven Redox Reactions in BIMEVOX-Type Phases. *Chem. Mater.* **2001**, *13* (2), 500–507.
(25) Arroyo y de Dompablo, M. E.; García-Alvarado, F.; Morán, E. Bi4V2O11 and Related Compounds as Positive Electrode Materials for Lithium Rechargeable Batteries. *Solid State Ion.* **1996**, *91* (3), 273–278.
(26) Débart, A.; Revel, B.; Dupont, L.; Montagne, L.; Leriche, J.-B.; Touboul, M.; Tarascon, J.-M. Study of the Reactivity Mechanism of M3B2O6 (with M= Co, Ni, and Cu) toward Lithium. *Chem. Mater.* **2003**, *15* (19), 3683–3691.

(27) Grey, C. P.; Dupré, N. NMR Studies of Cathode Materials for Lithium-Ion Rechargeable Batteries. *Chem. Rev.* **2004**, *104* (10), 4493–4512.
(28) Jiang, M.; Key, B.; Meng, Y. S.; Grey, C. P. Electrochemical and Structural Study of the Layered, "Li-Excess" Lithium-Ion Battery Electrode Material Li[Li1/9Ni1/3Mn5/9]O2. *Chem. Mater.* **2009**, *21* (13), 2733–2745.
(29) Rosina, K. J.; Jiang, M.; Zeng, D.; Salager, E.; Best, A. S.; Grey, C. P. Structure of Aluminum Fluoride Coated Li[Li1/9Ni1/3Mn5/9]O2 Cathodes for Secondary Lithium-Ion Batteries. *J. Mater. Chem.* **2012**, *22* (38), 20602–20610.
(30) Trease, N. M.; Seymour, I. D.; Radin, M. D.; Liu, H.; Liu, H.; Hy, S.; Chernova, N.; Parikh, P.; Devaraj, A.; Wiaderek, K. M.; Chupas, P. J.; Chapman, K. W.; Whittingham, M. S.; Meng, Y. S.; Van der Van, A.; Grey, C. P. Identifying the Distribution of Al3+ in LiNi0.8Co0.15Al0.05O2. *Chem. Mater.* **2016**, *28* (22), 8170–8180.
(31) Key, B.; Bhattacharyya, R.; Morcrette, M.; Seznéc, V.; Tarascon, J.-M.; Grey, C. P. Real-Time NMR Investigations of Structural Changes in Silicon Electrodes for Lithium-Ion Batteries. *J. Am. Chem. Soc.* **2009**, *131* (26), 9239–9249.
(32) Grey, C. P.; Tarascon, J. M. Sustainability and in Situ Monitoring in Battery Development. *Nat. Mater.* **2017**, *16* (1), 45–56.
(33) Li, Y.; Trujillo, M. A.; Fu, E.; Patterson, B.; Fei, L.; Xu, Y.; Deng, S.; Smirnov, S.; Luo, H. Bismuth Oxide: A New Lithium-Ion Battery Anode. *J. Mater. Chem. A* **2013**, *1* (39), 12123.
(34) Park, C.-M.; Yoon, S.; Lee, S.-I.; Sohn, H.-J. Enhanced Electrochemical Properties of Nanostructured Bismuth-Based Composites for Rechargeable Lithium Batteries. *J. Power Sources* **2009**, *186* (1), 206–210.
(35) Chagnes, A.; Swiatowska, J. Electrolyte and Solid-Electrolyte Interphase Layer in Lithium-Ion Batteries. In *Lithium Ion Batteries-New Developments*; InTech, 2012.
(36) Renman, V.; Hu, S.; Eriksson, R.; Maibach, J.; Johnsson, M.; Pay Gómez, C.; Edström, K. $Ni_3Sb_4O_6F_6$ and Its Electrochemical Behavior toward Lithium—A Combination of Conversion and Alloying Reactions. *Chem. Mater.* **2016**, *28* (18), 6520–6527.
(37) Sammes, N. M.; Tompsett, G. A.; Näfe, H.; Aldinger, F. Bismuth Based Oxide Electrolytes—Structure and Ionic Conductivity. *J. Eur. Ceram. Soc.* **1999**, *19* (10), 1801–1826.
(38) Skinner, S. J.; Kilner, J. A. Oxygen Ion Conductors. *Mater. Today* **2003**, *6* (3), 30–37.
(39) Kitada, A.; Hasegawa, G.; Kobayashi, Y.; Kanamori, K.; Nakanishi, K.; Kageyama, H. Selective Preparation of Macroporous Monoliths of Conductive Titanium Oxides TinO2n–1 (N = 2, 3, 4, 6). *J. Am. Chem. Soc.* **2012**, *134* (26), 10894–10898.
(40) Forni, L.; Fornasari, G.; Tosi, C.; Trifirò, F.; Vaccari, A.; Dumeignil, F.; Grimblot, J. Non-Conventional Sol–gel Synthesis for the Production of Boron-Alumina Catalyst Applied to the Vapour Phase Beckmann Rearrangement. *Appl. Catal. Gen.* **2003**, *248* (1–2), 47–57.
(41) Chen, K.; Ai, N.; Lievens, C.; Love, J.; Jiang, S. P. Impact of Volatile Boron Species on the Microstructure and Performance of Nano-Structured (Gd,Ce)O2 Infiltrated (La,Sr)MnO3 Cathodes of Solid Oxide Fuel Cells. *Electrochem. Commun.* **2012**, *23*, 129–132.
(42) Chen, K.; Hyodo, J.; O'Donnell, K. M.; Rickard, W.; Ishihara, T.; Jiang, S. P. Effect of Volatile Boron Species on the Electrocatalytic Activity of Cathodes of Solid Oxide Fuel Cells III. Ba0.5Sr0.5Co0.8Fe0.2O3-δ Electrodes. *J. Electrochem. Soc.* **2014**, *161* (12), F1163–F1170.
(43) Ibarra-Palos, A.; Darie, C.; Proux, O.; Hazemann, J. L.; Aldon, L.; Jumas, J. C.; Morcrette, M.; Strobel, P. Electrochemical Reactions of Iron Borates with Lithium: Electrochemical and in Situ Mössbauer and X-Ray Absorption Studies. *Chem. Mater.* **2002**, *14* (3), 1166–1173.
(44) Kim, H.; Kim, H.; Kim, H.; Kim, J.; Yoon, G.; Lim, K.; Yoon, W.-S.; Kang, K. Understanding Origin of Voltage Hysteresis in Conversion Reaction for Na Rechargeable Batteries: The Case of Cobalt Oxides. *Adv. Funct. Mater.* **2016**, *26* (28), 5042–5050.
(45) Yu, H.-C.; Ling, C.; Bhattacharya, J.; Thomas, J. C.; Thornton, K.; Van der Ven, A. Designing the next Generation High Capacity Battery Electrodes. *Energy Environ. Sci.* **2014**, *7* (5), 1760.
(46) Kamitsos, E. I.; Chryssikos, G. D. Borate Glass Structure by Raman and Infrared Spectroscopies. *J. Mol. Struct.* **1991**, *247*, 1–16.

(47) Konijnendijk, W. L.; Stevels, J. The Structure of Borate Glasses Studied by Raman Scattering. *J. Non-Cryst. Solids* **1975**, *18* (3), 307–331.
(48) Tuller, H. L.; Button, D. P.; Uhlmann, D. R. Fast Ion Transport in Oxide Glasses. *J. Non-Cryst. Solids* **1980**, *40* (1–3), 93–118.
(49) SClIUTT, H.-J. Wolfgang MULLER, Detlef KRUSCHKE, Manfred TORGE, Arnd-Rtidiger GRIMMER. *Solid State Ion.* **1987**, *23*, 53–58.

TOC graphic

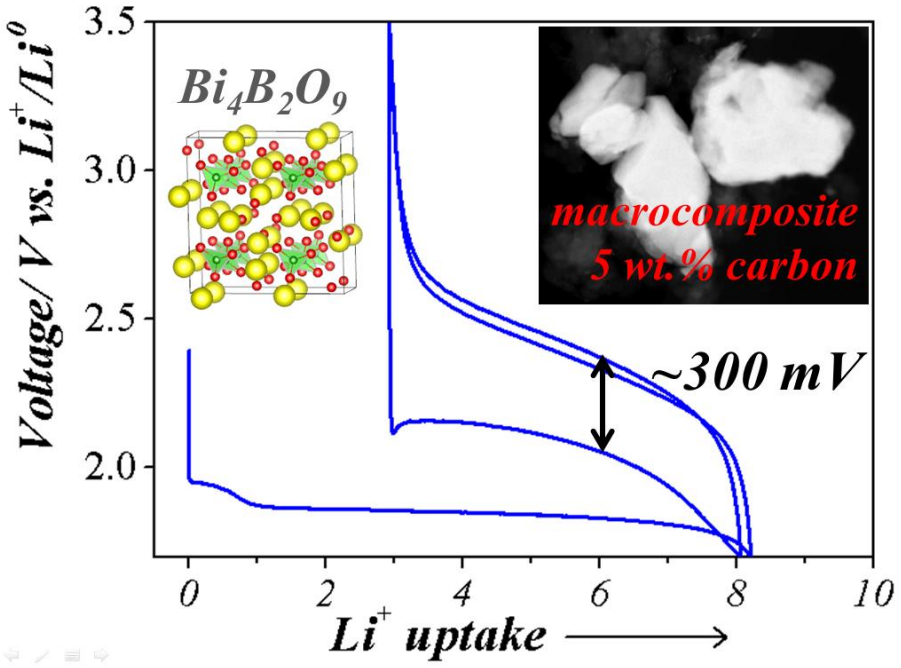

Galvanostatic charge-discharge curve for a $Bi_4B_2O_9$/C macrocomposite, highlighting the small voltage hysteresis for the conversion reaction around 300 mV.